

Purcell effect with microwave drive: Suppression of qubit relaxation rate

Eyob A. Sete¹, Jay M. Gambetta², and Alexander N. Korotkov¹

¹*Department of Electrical Engineering, University of California, Riverside, California 92521, USA*

²*IBM T.J. Watson Research Center, Yorktown Heights, New York 10598, USA*

(Dated: March 24, 2014)

We analyze the Purcell relaxation rate of a superconducting qubit coupled to a resonator, which is coupled to a transmission line and pumped by an external microwave drive. Considering the typical regime of the qubit measurement, we focus on the case when the qubit frequency is significantly detuned from the resonator frequency. Surprisingly, the Purcell rate decreases when the strength of the microwave drive is increased. This suppression becomes significant in the nonlinear regime. In the presence of the microwave drive, the loss of photons to the transmission line also causes excitation of the qubit; however, the excitation rate is typically much smaller than the relaxation rate. Our analysis also applies to a more general case of a two-level quantum system coupled to a cavity.

PACS numbers: 03.67.Lx, 03.65.Yz, 42.50.-p, 85.25.-j

I. INTRODUCTION

The spontaneous emission rate of an atom depends on the environment with which it is coupled. Changing the atom environment substantially alters the density of states, leading to suppression or enhancement of the spontaneous emission rate. This phenomenon was first predicted by Purcell in his seminal work [1]. When the atom is coupled on-resonance with a cavity, its relaxation rate is enhanced [1, 2] due to increased vacuum fluctuations at the atom frequency. On the other hand, if the atom is off-resonant from the cavity frequency, the spontaneous emission rate can be significantly suppressed [3–5].

A very similar effect [6] (thus often called the Purcell effect) occurs in circuit quantum electrodynamics (QED) systems [7, 8] when a superconducting qubit (artificial atom) is coupled to a microwave resonator, which in turn is coupled to a transmission line. The qubit energy relaxation via the resonator is one of the main processes limiting the qubit lifetime. As demonstrated experimentally [9], even coupling with resonator modes that are far detuned from the qubit frequency can significantly reduce the qubit lifetime. The Purcell effect is also one of the limiting factors in achieving a high-fidelity qubit readout. Several proposals have been put forward to reduce or eliminate the resonator-induced qubit relaxation rate (Purcell rate) either by designing a Purcell filter [10, 11], engineering a Purcell-protected qubit [12], or using a tunable coupler [13] that decouples the transmission line from the resonator during the qubit-resonator interaction, thereby avoiding the Purcell effect altogether [14].

In this work, we analyze the effect of an external microwave drive on the qubit relaxation rate caused by the loss of photons to the resonator environment. It is known [15, 16] that the external drive can increase the qubit relaxation rate (and also cause qubit excitation) due to the “dressed dephasing” effect, which essentially converts pure dephasing into photon-number-dependent

energy relaxation (the dressed dephasing was observed experimentally [17]). In our analysis we assume the absence of pure dephasing, so that there is no dressed dephasing, and we can focus on the question of how the standard Purcell effect changes in the presence of an additional drive. In spite of the general importance of this question, we are not aware of any direct discussion of the Purcell effect in the presence of drive, except for an indirect analysis in Ref. [16].

We consider a superconducting qubit coupled to a resonator, which can leak photons into a transmission line (Fig. 1). The resonator is driven on resonance by an external microwave field, while the qubit is significantly detuned from the resonator frequency, so that there is no direct effect of the drive on the qubit. Nevertheless, the presence of microwave photons in the resonator (with average number \bar{n}) may affect the qubit relaxation rate. Naively, we might expect that the qubit relaxation rate should scale approximately as $\bar{n} + 1$ with increasing drive, because the effective interaction between the qubit and resonator scales as $\sqrt{N_e}$, where N_e is the number of excitations in the system. However, this is not correct: the Purcell rate does not increase with \bar{n} . It is easy to understand this fact using a picture of an almost linear interaction between the qubit and resonator, so that the photons at the resonator frequency do not affect the evolution of the qubit excitation, which is at the qubit frequency. Our calculations confirm that the Purcell rate does not increase with \bar{n} even in the strongly nonlinear regime (when $\bar{n} \gtrsim n_{\text{crit}}$, where n_{crit} is the so-called critical photon number [7] – see later).

In fact, somewhat surprisingly, we find the opposite effect: the qubit decay rate *decreases* with increasing \bar{n} . This follows from an analytic formula, obtained in a simple intuitive approach. In the slightly nonlinear regime (when $\bar{n} \ll n_{\text{crit}}$) this formula is confirmed using a formal approach based on a dispersive expansion of the interaction Hamiltonian; the formula is also confirmed by a numerical simulation in a wider range of nonlinearity. The suppression of the relaxation rate becomes significant (it

may exceed an order of magnitude) when increasing \bar{n} brings the interaction into the strongly nonlinear regime ($n \gtrsim n_{\text{crit}}$). We have also found that besides the energy relaxation, in the presence of the microwave drive, the qubit may experience excitation as a result of photon loss to the resonator environment. In the moderately nonlinear regime the excitation rate grows with \bar{n} , but remains much smaller than the relaxation rate. The simple analytics and formal analysis for the relaxation as well as the excitation rate agree well with the numerical results.

The paper is organized in the following way. In Sec. II we start with reviewing the standard Purcell effect in the absence of a microwave drive. Then, in Sec. III, we calculate the Purcell rate in the presence of the drive analytically in two ways: using a simple approach and using a formal master equation approach. The analytical results are compared with the numerical results in Sec. IV. Finally, Sec. V is the conclusion.

II. PURCELL EFFECT WITHOUT DRIVE

We begin with a discussion of the Purcell rate calculation [18] by considering a qubit coupled to a resonator in the absence of a microwave drive. In this case, there are only three (bare) states involved in the evolution: $|e\rangle = |e\rangle|0\rangle = |e, 0\rangle$, $|1\rangle = |g\rangle|1\rangle = |g, 1\rangle$, and $|g\rangle = |g\rangle|0\rangle = |g, 0\rangle$, where $|e\rangle$ and $|g\rangle$ denote the qubit states, while $|0\rangle$ or $|1\rangle$ represents the resonator state with 0 or 1 photon. We assume that the system is initially in the state $|e\rangle$ or a superposition of $|e\rangle$ and $|1\rangle$. Then the qubit-resonator coupling causes coherent oscillations between the states $|e\rangle$ and $|1\rangle$; however, leakage of the photon to the resonator environment eventually causes irreversible relaxation to the system ground state $|g\rangle$ (note that in some cases the Purcell relaxation can be considered as a coherent process [19]).

The qubit-resonator system is described by the usual Jaynes-Cummings (JC) Hamiltonian ($\hbar = 1$)

$$H = \omega_r a^\dagger a + \frac{1}{2} \omega_q \sigma_z + g(a^\dagger \sigma_- + a \sigma_+), \quad (1)$$

where ω_r and ω_q are the resonator and the qubit frequencies, respectively, and g is the qubit-resonator coupling, assumed to be real for simplicity of notations. Here σ_\pm are the qubit raising and lowering operators, $\sigma_z = |e\rangle\langle e| - |g\rangle\langle g| = \sigma_+ \sigma_- - \sigma_- \sigma_+$, and a (a^\dagger) is the annihilation (creation) operator for the resonator field.

Let us use the rotating frame, which rotates with frequency ω_r for both the resonator and qubit. Formally, this is introduced by using the interaction picture, based on separating the Hamiltonian into two parts, $H = H_0 + V$, with

$$H_0 = \omega_r a^\dagger a + \frac{1}{2} \omega_q \sigma_z, \quad (2)$$

$$V = \frac{\Delta}{2} \sigma_z + g(a^\dagger \sigma_- + a \sigma_+), \quad (3)$$

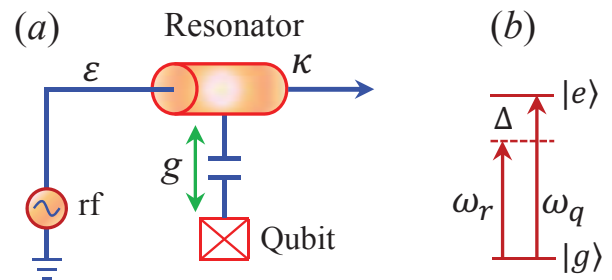


FIG. 1. (a) Schematic of the considered system with (b) the energy-level diagram. The qubit is off-resonantly ($\Delta = \omega_q - \omega_r$) coupled to the resonator, with coupling constant g . The resonator decays with the rate κ , which causes the energy relaxation (Purcell relaxation) of the qubit. In a circuit QED qubit measurement setup, a microwave (rf) drive with resonant frequency ω_r and normalized amplitude ϵ is applied to the resonator. We show that the qubit relaxation rate decreases with increasing strength of this drive, and that there exists a relatively weak qubit excitation.

where $\Delta = \omega_q - \omega_r$, H_0 is the free Hamiltonian, and V is the remaining interaction part. Note however that in the interaction picture the Hamiltonian does not depend on time, $V_I = \exp(iH_0 t) V \exp(-iH_0 t) = V$, because V commutes with H_0 . Even though the resonator and qubit operators now formally depend on time, $a(t) = a(0) \exp(-i\omega_r t)$, $a^\dagger(t) = a(0) \exp(i\omega_r t)$, and $\sigma_\pm(t) = \sigma_\pm(0) \exp(\pm i\omega_r t/2)$, they always come in pairs, so that the time dependence is canceled out. This is why we can still use the time-independent operators a , a^\dagger , and σ_\pm , which simplifies calculations. This trick is possible because the JC Hamiltonian (1) is only the rotating-wave approximation of the actual physical Hamiltonian.

The evolution of the qubit-resonator system that accounts for the photon loss from the resonator can be described by a master equation in Lindblad form [18]

$$\dot{\rho} = -i[V, \rho] + \kappa \mathcal{D}[a]\rho, \quad (4)$$

$$\kappa \mathcal{D}[a]\rho = \kappa(a\rho a^\dagger - a^\dagger a\rho/2 - \rho a^\dagger a/2), \quad (5)$$

where κ is the resonator decay rate. Note that as discussed above, all operators here (except the density matrix ρ) do not depend on time, even though we are using the interaction picture. Also note that in this master equation we assumed that coupling between the resonator and the bath (transmission line) is frequency-independent; this assumption is no longer valid in the case of the Purcell filter [10, 11], when κ becomes frequency-dependent.

Since we are only interested in quantifying the qubit relaxation through the resonator, we do not take into account the intrinsic qubit relaxation and pure dephasing. Using Eq. (4), one easily obtains the equations for the density matrix elements in the single-excitation subspace (in the bare-state basis of $|e\rangle$ and $|1\rangle$), which are

decoupled from the elements containing state $|\mathbf{g}\rangle$,

$$\begin{pmatrix} \dot{\rho}_{ee} \\ \dot{\rho}_{11} \\ \dot{\rho}_{e1}^- \\ \dot{\rho}_{e1}^+ \end{pmatrix} = \begin{pmatrix} 0 & 0 & ig & 0 \\ 0 & -\kappa & -ig & 0 \\ 2ig & -2ig & -\frac{\kappa}{2} & -i\Delta \\ 0 & 0 & -i\Delta & -\frac{\kappa}{2} \end{pmatrix} \begin{pmatrix} \rho_{ee} \\ \rho_{11} \\ \rho_{e1}^- \\ \rho_{e1}^+ \end{pmatrix}, \quad (6)$$

where $\rho_{e1}^\pm = \rho_{e1} \pm \rho_{1e}$. Here the bare-state populations ρ_{ee} and ρ_{11} are coupled to the coherences ρ_{e1}^\pm via terms proportional to g , while the damping term proportional to κ contributes to the decay of ρ_{11} , but does not affect ρ_{ee} . Note that the coherences ρ_{e1}^\pm decay with the rate $\kappa/2$. The population of the state $|\mathbf{g}\rangle$ obviously increases as $\dot{\rho}_{gg} = \kappa\rho_{11}$. Equation (6) can be used in numerical as well as in analytical calculations. In particular, the eigenvalues of the evolution can be found analytically from the corresponding quartic equation, which in this case has a relatively simple solution. Below we will obtain these eigenvalues in a different way.

Instead of using the density matrix language for the description of the Purcell effect, it is also possible to use the simpler language of wavefunctions, even in the presence of the decay κ . Physically, this is because in the single-excitation subspace unraveling of the Lindblad equation (see, e.g., [20]) corresponds to only one scenario with no relaxation, and therefore the wavefunction evolution is non-stochastic. More formally, we can rewrite the master equation (4) as [21, 22] $\dot{\rho} = -i[H_{\text{eff}}, \rho] + \kappa\rho a^\dagger$, where $H_{\text{eff}} = V - i\kappa a^\dagger a/2$ is an effective non-Hermitian Hamiltonian. The term $\kappa\rho a^\dagger$ can be neglected because in the single-excitation subspace it produces a contribution only from higher-excitation subspaces, which are not populated. Therefore, in the single-excitation subspace we have $\dot{\rho} = -i[H_{\text{eff}}, \rho]$ or equivalently $|\dot{\psi}\rangle = -iH_{\text{eff}}|\psi\rangle$, which describes the evolution of the *decaying* wavefunction $|\psi(t)\rangle = \alpha(t)|\mathbf{e}\rangle + \beta(t)|\mathbf{1}\rangle$:

$$\dot{\alpha} = -i\frac{\Delta}{2}\alpha - ig\beta, \quad (7)$$

$$\dot{\beta} = i\frac{\Delta}{2}\beta - ig\alpha - \frac{\kappa}{2}\beta. \quad (8)$$

(Another way to derive these equations is by considering only the no-relaxation scenario when unraveling the evolution [20].) These are the usual equations for a two-level system, but with complex energy $-\Delta/2 - i\kappa/2$ of the bare state $|\mathbf{1}\rangle$. Using the standard diagonalization procedure, we can find two eigenstates with energies $\tilde{E} = -i\kappa/4 \pm \sqrt{-\kappa^2/16 + g^2 + \Delta^2/4 + i\kappa\Delta/4}$, which can be written as

$$\tilde{E}_e = \frac{\Omega}{2} - i\frac{\Gamma}{2}, \quad \tilde{E}_1 = -\frac{\Omega}{2} - i\frac{\kappa - \Gamma}{2}, \quad (9)$$

with

$$\Gamma = \frac{\kappa}{2} - \frac{\sqrt{2}}{2} \sqrt{-A + \sqrt{A^2 + (\kappa\Delta)^2}}, \quad (10)$$

$$\Omega = \frac{\sqrt{2}}{2} \sqrt{A + \sqrt{A^2 + (\kappa\Delta)^2}} \text{sgn}(\Delta), \quad (11)$$

$$A = \Delta^2 + 4g^2 - \kappa^2/4. \quad (12)$$

Here \tilde{E}_e is the complex energy of the eigenstate (“dressed” state, which includes decay), corresponding to the excited qubit, while \tilde{E}_1 corresponds to the dressed resonator photon (notice the sign of Δ in the formula for Ω). Since $\text{Im}(\tilde{E}_e) = -\Gamma/2$, the population of the qubit dressed state decays with the rate Γ . Therefore Γ is the qubit relaxation rate, i.e., the Purcell rate, while the photon relaxation rate is $\kappa - \Gamma$. If the initial state is not one of these eigenstates, then the evolution also includes oscillations with beating frequency Ω , decaying with the rate $-\text{Im}(\tilde{E}_e + \tilde{E}_1) = \kappa/2$. We have checked that the same rates can be obtained by diagonalizing the evolution matrix in Eq. (6), which has four eigenvalues: $-\Gamma$, $-(\kappa - \Gamma)$, and $-\kappa/2 \pm i\Omega$, as expected from Eq. (9). Note that for small κ the frequency $|\Omega|$ is close to the usual Rabi frequency $\sqrt{\Delta^2 + 4g^2}$, but large κ may change it significantly.

The eigenstates (dressed states with decay) $|\tilde{\mathbf{e}}\rangle = \tilde{\alpha}_e|\mathbf{e}\rangle + \tilde{\beta}_e|\mathbf{1}\rangle$ and $|\tilde{\mathbf{1}}\rangle = \tilde{\alpha}_1|\mathbf{e}\rangle + \tilde{\beta}_1|\mathbf{1}\rangle$ corresponding to the energies \tilde{E}_e and \tilde{E}_1 can be found in the standard way, via the ratio $\tilde{\beta}_{e,1}/\tilde{\alpha}_{e,1} = (\tilde{E}_{e,1} - \Delta/2)/g$ and the normalization condition. However, note that these eigenstates are not mutually orthogonal, so finding the expansion of an initial state in the eigenbasis, $|\psi_{\text{in}}\rangle = \tilde{c}_e|\tilde{\mathbf{e}}\rangle + \tilde{c}_1|\tilde{\mathbf{1}}\rangle$, is somewhat more involved: $\tilde{c}_1 = \langle \tilde{\mathbf{e}}_\perp | \psi_{\text{in}} \rangle / \langle \tilde{\mathbf{e}}_\perp | \tilde{\mathbf{1}} \rangle$, where $|\tilde{\mathbf{e}}_\perp\rangle$ is the vector orthogonal to $|\tilde{\mathbf{e}}\rangle$ (similarly for \tilde{c}_e). The evolution in the single-excitation subspace is then $|\psi(t)\rangle = \tilde{c}_e e^{-i\Omega t/2} e^{-\Gamma t/2} |\tilde{\mathbf{e}}\rangle + \tilde{c}_1 e^{i\Omega t/2} e^{-(\kappa - \Gamma)t/2} |\tilde{\mathbf{1}}\rangle$, and it is easy to find the density matrix elements; for example the bare-state qubit occupation is $\rho_{ee}(t) = |\tilde{c}_e \tilde{\alpha}_e e^{-i\Omega t/2} e^{-\Gamma t/2} + \tilde{c}_1 \tilde{\alpha}_1 e^{i\Omega t/2} e^{-(\kappa - \Gamma)t/2}|^2$.

Now let us consider several special cases starting with the case usually discussed for optical systems (e.g., [18]), in which the resonator damping rate is much larger than the coupling: $\kappa \gg |g|$, while Δ is arbitrary. Expanding Eqs. (10) and (11) in g/κ and keeping the first two leading terms produces

$$\Gamma = \frac{\kappa g^2}{\Delta^2 + (\kappa/2)^2}, \quad (13)$$

$$\Omega = \Delta \left(1 + \frac{2g^2}{\Delta^2 + (\kappa/2)^2} \right). \quad (14)$$

This formula for the Purcell rate Γ can be interpreted as Fermi’s golden rule for the transition from the state $|\mathbf{e}\rangle$ to the relaxation-widened state $|\mathbf{1}\rangle$ with width κ . Note that at resonance, $\Delta = 0$, the Purcell rate (13) reduces to $\Gamma = 4g^2/\kappa$, while in the case $|\Delta| \gg \kappa$ it becomes $\Gamma = \kappa g^2/\Delta^2$; also note that $\Gamma \ll \kappa$ because of the assumption $|g| \ll \kappa$. If the evolution starts with the bare state $|\mathbf{e}\rangle$, then the probability to find the qubit in the excited state decays as

$$\rho_{ee}(t) \approx e^{-\Gamma t} \left[1 + \frac{8g^2(\kappa^2 - 4\Delta^2)}{(\kappa^2 + 4\Delta^2)^2} \right] - \frac{8g^2 e^{-\kappa t/2}}{(\kappa^2 + 4\Delta^2)^2} \times [4\kappa|\Delta| \sin(|\Omega|t) + (\kappa^2 - 4\Delta^2) \cos(\Omega t)]. \quad (15)$$

In this formula the oscillation amplitude is always small because of the assumption $|g| \ll \kappa$ (the amplitude of

the neglected term $e^{-(\kappa-\Gamma)t}$ is even smaller), so that in the leading order $\rho_{ee}(t) \approx e^{-\Gamma t}$. We have obtained Eq. (15) from the density matrix evolution (6) by using the method of Laplace transform, in which $\rho(t) \rightarrow \rho(s)$ and $\dot{\rho}(t) \rightarrow s\rho(s) - \rho(t=0)$. The solution is then obtained by taking the inverse Laplace transform of $\rho(s)$.

In circuit QED experiments the typical regime is different from what is usually considered in optics. Most importantly, instead of the above assumption $\kappa \gg |g|$, in the circuit QED systems the relation is usually the opposite: $\kappa \lesssim |g|$ or even $\kappa \ll |g|$. Therefore, the result (13) for the Purcell rate is inapplicable in the way we derived it, but we can still use the exact formula (10). [Note that Eq. (13) can actually be derived from Eq. (10) using a weaker assumption: $|g| \ll \max(\kappa, |\Delta|)$.] The formula for the Purcell rate that is most widely used in the circuit QED is the strong-dispersive-regime formula [7]

$$\Gamma_d = \frac{\kappa g^2}{\Delta^2}, \quad (16)$$

which can be derived from Eq. (10) by assuming $|\Delta| \gg \max(|g|, \kappa)$, keeping the relation between $|g|$ and κ arbitrary. This formula has a simple interpretation: the fraction $(g/\Delta)^2$ of the dressed qubit state (i.e. the eigenstate) is in the form of the resonator photon, and this part decays with the rate κ .

Now let us derive the expression for the Purcell rate using the weaker assumption $\kappa \ll \sqrt{\Delta^2 + 4g^2}$, which is usually well-satisfied in the circuit QED experiments. The detuning $|\Delta|$ may be much larger or comparable to the coupling $|g|$. In this case it is physically natural to use the basis of the single-excitation eigenstates (dressed states without decay) $|\overline{e}, 0\rangle$ and $|\overline{g}, 1\rangle$ besides the basis of the bare states $|\mathbf{e}\rangle = |e, 0\rangle$ and $|\mathbf{1}\rangle = |g, 1\rangle$. (Note the difference from the eigenbasis $\{|\tilde{\mathbf{e}}\rangle, |\tilde{\mathbf{1}}\rangle\}$, which includes decay.) If the initial state is $|\overline{e}, 0\rangle$, then the system would remain in this state if $\kappa = 0$. However, non-zero (but still small) κ causes the rare jumps $|\overline{g}, 1\rangle \rightarrow |g, 0\rangle$. Therefore, the rate of jumps should be proportional to the occupation of the bare state $|g, 1\rangle$ and the Purcell rate can be approximated as

$$\Gamma_P = \kappa |\langle g, 1 | \overline{e}, 0 \rangle|^2 = \frac{\kappa}{2} \left(1 - \frac{\Delta}{\sqrt{\Delta^2 + 4g^2}} \right), \quad (17)$$

where we used the exact formula for the overlap between the states $|\overline{e}, 0\rangle$ and $|g, 1\rangle$. Numerical comparison between this formula and exact result (10) shows that it is a very good approximation for small κ ; in particular, the relative error is less than $0.25\kappa^2/(\Delta^2 + 4g^2)$ for $\kappa/g < 4$. We will be using Eq. (17) in the following sections. It is easy to see that in the regime $|\Delta| \gg |g|$ the rate Γ_P reduces to Γ_d in Eq. (16).

If the evolution starts with the bare state $|e, 0\rangle$, then in the dispersive regime, $|\Delta| \gg |g| \gtrsim \kappa$, its population evolves as

$$\rho_{ee}(t) \approx e^{-\Gamma_P t} \left(1 - \frac{2g^2}{\Delta^2} \right) + \frac{2g^2}{\Delta^2} \cos(\Omega t) e^{-\kappa t/2}, \quad (18)$$

where $|\Omega| \approx \sqrt{\Delta^2 + 4g^2}$. The oscillation amplitude is small, but still noticeable for moderate values of Δ/g . In contrast, if the evolution starts with the eigenstate $|\overline{e}, 0\rangle$, then the population of this eigenstate decays almost without oscillation,

$$\overline{\rho}_{ee} \approx e^{-\Gamma_P t} \left(1 + \frac{g^2 \kappa^2}{2\Delta^4} \right) - \frac{g^2 \kappa^2}{2\Delta^4} \cos(\Omega t) e^{-\kappa t/2} \approx e^{-\Gamma_P t}. \quad (19)$$

The small remaining oscillation amplitude $g^2 \kappa^2 / 2\Delta^4$ is due to the difference between $|\overline{e}, 0\rangle$ and $|\tilde{\mathbf{e}}\rangle$, while the amplitude $2g^2/\Delta^2$ in Eq. (18) is due to the much larger difference between $|e, 0\rangle$ and $|\overline{e}, 0\rangle$ (the factor of 2 comes from two conversions: from the bare basis to the eigenbasis and then back).

III. PURCELL EFFECT WITH MICROWAVE DRIVE

So far we have only considered one excitation in the system. This situation is relevant to the qubit decay during coherent operations in circuit QED systems. However, the qubit measurement [7, 23–25] requires adding a microwave drive in resonance (or close to resonance) with the resonator frequency – see Fig. 1. This is the main motivation here to analyze qubit relaxation through the resonator in the presence of additional excitations in the system. To this end, we consider a dispersive qubit-resonator interaction (but not necessarily strongly dispersive, say $|\Delta/g| \geq 5$) with an external microwave drive. The Hamiltonian for the qubit-resonator system with a coherent microwave drive is given by

$$H = \omega_r a^\dagger a + \frac{1}{2} \omega_q \sigma_z + g(a^\dagger \sigma_- + a \sigma_+) + \varepsilon (a e^{i\omega_d t} + a^\dagger e^{-i\omega_d t}), \quad (20)$$

where ω_d is the drive frequency and ε , assumed to be real and constant, is the normalized amplitude of the microwave drive.

Following the same line of reasoning as was used to derive Eq. (4), we introduce the frame rotating at ω_r via the free Hamiltonian (2), so that the interaction part of the Hamiltonian in this frame has the form

$$H_I = \frac{\Delta}{2} \sigma_z + g(a^\dagger \sigma_- + a \sigma_+) + \varepsilon \left(e^{i(\omega_d - \omega_r)t} a + e^{-i(\omega_d - \omega_r)t} a^\dagger \right), \quad (21)$$

where all operators are time-independent. For simplicity we assume the drive to be exactly on resonance with the resonator frequency, $\omega_d = \omega_r$, though this assumption is not critical for our analysis. The master equation, including the loss of photons through the resonator [see Eq. (5)], is given by

$$\dot{\rho} = -i[H_I, \rho] + \kappa \mathcal{D}[a]\rho. \quad (22)$$

We focus on the experimentally important regime of sufficiently small resonator damping rate, $\kappa \ll |\Delta|$. More precisely, we assume $\kappa \ll \sqrt{\Delta^2 + 4g^2(\bar{n} + 1)}$, where \bar{n} is the average number of photons in the resonator, induced by the drive. In this case the Jaynes-Cummings ladder of levels [26] (Fig. 2) is affected by an interaction (between $|e, n\rangle$ and $|g, n+1\rangle$) with the strength $\sqrt{N_e}g$, but the effect of κ is relatively small. Here N_e is the total number of excitations, $N_e = n$ for the bare state $|g, n\rangle$ and $N_e = n + 1$ for the state $|e, n\rangle$. Therefore, it is natural to introduce the basis of the pairwise eigenstates represented by red dashed lines in Fig. 2 and denoted by the overline:

$$\overline{|e, n\rangle} = \cos \theta_{n+1} |e, n\rangle - \sin \theta_{n+1} |g, n+1\rangle, \quad (23)$$

$$\overline{|g, n\rangle} = \cos \theta_n |g, n\rangle + \sin \theta_n |e, n-1\rangle, \quad (24)$$

$$\tan(2\theta_n) = 2g\sqrt{\bar{n}}/\Delta. \quad (25)$$

The level splitting between the eigenstates is

$$\begin{aligned} \overline{E}_{e,n-1} - \overline{E}_{g,n} &= \sqrt{\Delta^2 + 4ng^2} \operatorname{sgn}(\Delta) \\ &= \Delta \sqrt{1 + 4N_e g^2 / \Delta^2}, \end{aligned} \quad (26)$$

and in the rotating frame, which we use, both energies are symmetric about zero, $\overline{E}_{g,n} = -\overline{E}_{e,n-1}$. Note that the level splitting changes significantly when the number of photons n becomes comparable with the so-called critical photon number [7],

$$n_{\text{crit}} = \frac{\Delta^2}{4g^2}. \quad (27)$$

The use of eigenstates as logical states in quantum computing applications is more natural than the use of the bare states [27], and in most practical cases the dynamics is sufficiently adiabatic to be naturally represented in the eigenbasis [14]. Therefore, when we will consider the qubit being initially in the excited state, we will actually assume that the initial state is the (coherent-state) superposition of *eigenstates* (23) corresponding to the excited state of the qubit (right set of red dashed lines in Fig. 2). Accordingly, the relaxation process corresponds to increasing occupation of the $|g\rangle$ -eigenstates (24) (left set of red dashed lines in Fig. 2). The use of eigenstates allows us to avoid oscillations in the evolution, caused by the difference between the bases [see, e.g., Eqs. (18) and (19) for the single-excitation case].

In the following, we present two ways to derive an approximate analytical formula for the Purcell rate in the presence of a microwave drive. We first use a simple intuitive approach applicable for an arbitrary nonlinearity (arbitrary ratio \bar{n}/n_{crit}) and then use a formal perturbative approach applicable in the slightly nonlinear regime ($\bar{n} \ll n_{\text{crit}}$). The results of the two approaches are shown to coincide in the validity range of the formal approach.

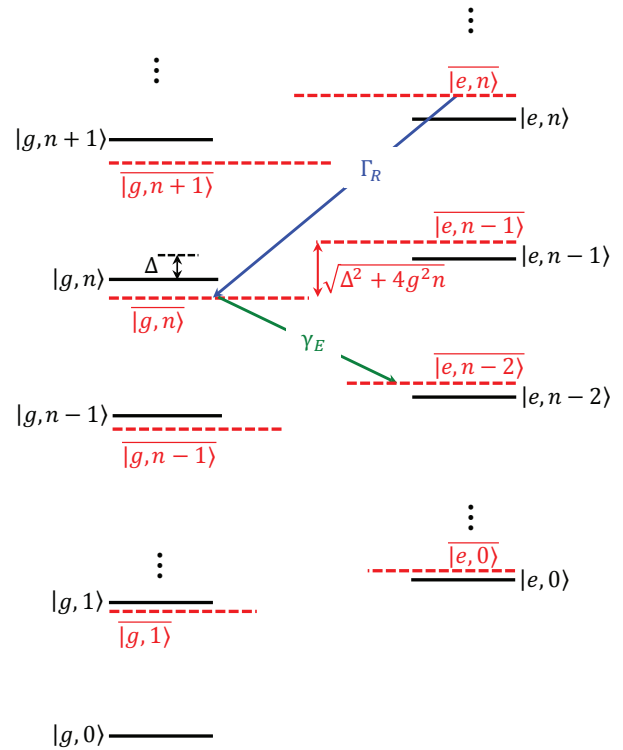


FIG. 2. The Jaynes-Cummings ladder in the bare-state basis (black solid lines) and the eigenstate basis (red dashed lines). Here transitions (“jumps”) from the right set to the left set of eigenstates correspond to qubit relaxation with rate Γ_R , while transitions from the left to the right set of eigenstates give rise to qubit excitation with rate γ_E .

A. Purcell rate with drive: Simple approach

The damping of the resonator state is described by the Lindblad form (5). We can think of this process by unraveling it into “jump” and “no jump” scenarios (see, e.g., [20]), so that the first term in Eq. (5) describes random jumps due to the action of the operator a , which occur with the rate $\kappa \operatorname{Tr}(a^\dagger \rho) = \kappa \bar{n}$, while the remaining two terms describe the state evolution due to absence of jumps. Without the qubit the driven resonator would reach a steady coherent state, for which the jump produces no change (because the coherent state is an eigenstate of the operator a), while the photon-number decay due to the no-jump evolution [20] is compensated by the drive. In the presence of the qubit there are two sets of eigenstates (Fig. 2, we will refer to them as two ladders) and within each ladder the process is approximately the same as without the qubit (up to a factor, accounting for the overall population of each ladder). However, the jumps *between* the ladders lead to Purcell-effect relaxation (or excitation).

Qubit relaxation rate

If the system is in the eigenstate $\overline{|e, n\rangle}$ (see Fig. 2), then the (random) action of the operator a gives the unnormalized state $a\overline{|e, n\rangle}$. This state is a superposition of bare states $|e, n-1\rangle$ and $|g, n\rangle$. Expanding the state $a\overline{|e, n\rangle}$ in the eigenbasis, we see that most of it contributes to $\overline{|e, n-1\rangle}$, which belongs to the set of excited eigenstates. However, there is a non-zero overlap between $a\overline{|e, n\rangle}$ and $\overline{|g, n\rangle}$, which leads to the qubit energy relaxation (transition from the right to left ladder of eigenstates in Fig. 2). The rate of this relaxation process [28] (Purcell rate from the state $\overline{|e, n\rangle}$) is therefore

$$\Gamma_R(n) = \kappa |\overline{\langle g, n | a | e, n \rangle}|^2, \quad (28)$$

where the subscript R means relaxation. Note that $\Gamma_R(0) = \Gamma_P$ [see Eq. (17)]. Using explicit expressions (23) and (24) for the eigenstates, we find

$$\Gamma_R(n) = \kappa (\sqrt{n+1} \sin \theta_{n+1} \cos \theta_n - \sqrt{n} \sin \theta_n \cos \theta_{n+1})^2, \quad (29)$$

where θ_n is given by Eq. (25).

It is important that there is a significant energy shift ($\simeq \sqrt{\Delta^2 + 4g^2\bar{n}}$) between the two ladders of eigenstates, so that the contribution to $\overline{|g, n\rangle}$ due to the next jump from $\overline{|e, n\rangle}$ is incoherent with the previous jump contribution (it brings a different random phase), which allows us to characterize the relaxation process by a rate Γ_R . However, when different eigenstates $\overline{|e, n\rangle}$ are populated, then the jumps from these states occur in a mutually coherent way (the operator a acts on the superposition), resulting in a mutual coherence within the set of eigenstates in the left ladder in Fig. 2. Nevertheless, this does not affect the jumps between the left and right ladders of states, and therefore the rate $\Gamma_R(n)$ can be simply averaged over the population $P(n)$ of the states $\overline{|e, n\rangle}$,

$$\Gamma_R = \left[\sum_{n=0}^{\infty} P(n) \Gamma_R(n) \right] / \sum_{n=0}^{\infty} P(n). \quad (30)$$

A natural assumption is that $P(n)$ is close to the coherent-state distribution (the normalization is not important),

$$P(n) = e^{-\bar{n}} \bar{n}^n / n!. \quad (31)$$

Actually, this coherent-state assumption becomes invalid at sufficiently large \bar{n} , when non-linearities (like squeezing) become significant; however, this is not important because at $\bar{n} \gg 1$ the averaging (30) is not really needed as long as the spread of occupied values of n is much smaller than \bar{n} . For \bar{n} , it is natural to use the value in the absence of qubit, $\bar{n} \approx 4|\epsilon|^2/\kappa^2$, or a more accurate value, which accounts for the shift of the resonator frequency by the qubit – see Eq. (71) later. Note that here \bar{n} is the average number of photons in the ladder of “excited” eigenstates (it would be better to use a different

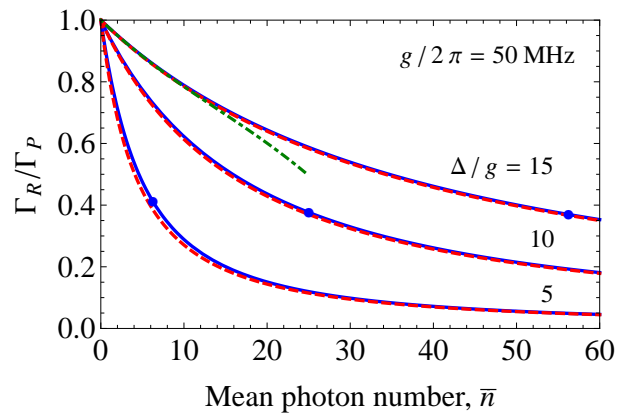


FIG. 3. The Purcell relaxation rate Γ_R normalized by the no-drive value Γ_P , as a function of the mean photon number \bar{n} induced by the drive for several values of normalized detuning Δ/g : 15, 10, and 5. The dashed red lines show $\Gamma_R(\bar{n})$ calculated using Eq. (29), the blue solid lines show Γ_R averaged over the coherent state distribution using Eq. (30). For the upper curve we also show the truncated expansion [up to λ^8 , Eq. (33)] by the green dot-dashed line. The blue dots on the lines indicate n_{crit} .

notation, \bar{n}_e , for this meaning – see the next subsection, but we will use \bar{n} here for brevity).

The blue solid lines in Fig. 3 show the \bar{n} -dependence of the Purcell rate Γ_R (normalized by the no-drive value Γ_P) for several values of the normalized detuning Δ/g . As we see, the Purcell rate decreases with increasing \bar{n} , and the suppression (compared with the no-drive case) can be strong at large \bar{n} . The dashed red lines show $\Gamma_R(\bar{n})$ calculated using Eq. (29), in which a non-integer \bar{n} is introduced in the natural way via a non-integer \bar{n} in Eq. (25). As expected, the dashed and solid lines almost coincide at $\bar{n} \gg 10$, while there is a noticeable difference between them for $\bar{n} \lesssim 10$ when Δ/g is not very large.

In the experimentally interesting regime when $\Delta \gg g$, the rate Γ_R can be expanded in powers of

$$\lambda = g/\Delta. \quad (32)$$

(We will need this expansion for comparison with the results of the formal approach in the next subsection.) Expanding Eq. (29) in powers of λ , we obtain $\Gamma_R(n) = \kappa \lambda^2 [1 - 3\lambda^2(2n+1) + \lambda^4(31n^2 + 31n + 10) - \lambda^6(150n^3 + 225n^2 + 145n + 35) + \dots]$. The averaging (30) then gives $\overline{n^2} = \bar{n}^2 + \bar{n}$, $\overline{n^3} = \bar{n}^3 + 3\bar{n}^2 + \bar{n}$, etc., thus resulting in a series

$$\Gamma_R = \kappa \lambda^2 [1 - 3\lambda^2(2\bar{n} + 1) + \lambda^4(31\bar{n}^2 + 62\bar{n} + 10) - \lambda^6(150\bar{n}^3 + 675\bar{n}^2 + 520\bar{n} + 35) + \dots]. \quad (33)$$

This truncated series is shown by the green dot-dashed line in Fig. 3.

The first term in the expansion (33) gives the standard Purcell rate $\Gamma_d = \kappa g^2/\Delta^2$ in the strong dispersive regime ($\lambda \ll 1$) – see Eq. (16). The negative sign of the second

term means that the Purcell rate decreases with increasing number of photons in the resonator. In the leading order of the correction (assuming $1 \ll \bar{n} \ll n_{\text{crit}}$) Eq. (33) becomes

$$\Gamma_R \approx \Gamma_d \left(1 - \frac{3}{2} \frac{\bar{n}}{n_{\text{crit}}} \right), \quad (34)$$

where n_{crit} is given by Eq. (27). Note that Eq. (34) gives a slightly inaccurate value for $\bar{n} \lesssim 1$ since at $\bar{n} = 0$ the expansion (33) gives $\Gamma_R(0) = \Gamma_P$ [see Eq. (17)]; however, the difference between Γ_d with Γ_P is small when $|g/\Delta| \ll 1$.

When $\bar{n} \gg 1$, we do not need the summation in Eq. (30) and can use approximation $\Gamma_R \approx \Gamma_R(\bar{n})$ if the effective spread of n values is much smaller than \bar{n} , i.e., $\sqrt{\bar{n}^2 - \bar{n}^2} \ll \bar{n}$ (therefore, moderate nonlinear effects still allow this simplification). In this case $|\theta_{\bar{n}+1} - \theta_{\bar{n}}| \ll 1$ in Eq. (29), and using the first-order expansion of this equation we obtain the approximation

$$\Gamma_R \approx \frac{\kappa g^2}{4\Delta^2} \left(\frac{1}{1 + \bar{n}/n_{\text{crit}}} + \frac{1}{\sqrt{1 + \bar{n}/n_{\text{crit}}}} \right)^2, \quad (35)$$

which is valid when $\bar{n} \gg 1$ with arbitrary ratio \bar{n}/n_{crit} . (This is in contrast to the truncated perturbative expansion in powers of λ , which works well only for $\bar{n}/n_{\text{crit}} \ll 1$.)

From Eq. (35) we see that the Purcell rate Γ_R decreases significantly when \bar{n} becomes comparable to n_{crit} , and it continues to decrease with increasing \bar{n} , eventually approaching zero. Figure 4 illustrates the dependence of the Purcell rate Γ_R (normalized by the no-drive value Γ_P) on the ratio \bar{n}/n_{crit} for several values of the normalized detuning Δ/g . We see that the different curves shown in Fig. 3 now collapse onto practically the same line for $|\Delta/g| \gtrsim 10$, with a significant deviation starting only when $|\Delta/g| \lesssim 5$. The approximation (35) is shown by the black dot-dashed line for large Δ/g . This approximation also works well (not shown) for the upper curve, $\Delta/g = 5$, except for the range $\bar{n} \lesssim 3$ (correspondingly $\bar{n}/n_{\text{crit}} \lesssim 0.5$), because of the difference between Γ_d and Γ_P . From Eq. (35), the suppression at $\bar{n} = n_{\text{crit}}$ is $\Gamma_R/\Gamma_P \approx (3 + 2\sqrt{2})/16 = 0.36$ for large Δ/g .

In the strong suppression limit when $\bar{n} \gg n_{\text{crit}}$, the rate (29) [or (35)] can be approximated as

$$\Gamma_R \approx \Gamma_d \frac{n_{\text{crit}}}{4\bar{n}} \left[1 + 2\sqrt{\frac{n_{\text{crit}}}{\bar{n}}} \right]. \quad (36)$$

This approximation and the opposite-limit approximation (34) are shown by red dashed lines in Fig. 4.

Qubit excitation rate

Similar to the calculation of the qubit energy relaxation rate (28), we can calculate the qubit excitation rate.

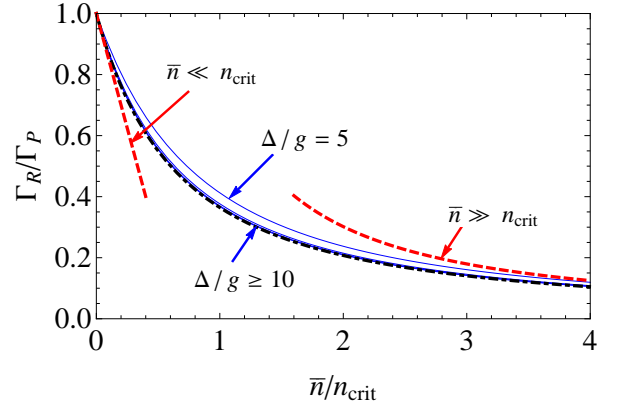


FIG. 4. The Purcell relaxation rate Γ_R [Eq. (30)] normalized by the no-drive value Γ_P [Eq. (17)] versus \bar{n}/n_{crit} for several values of Δ/g : 5, 10, 15, and 20 (blue solid lines). The curves for $\Delta/g \geq 10$ are practically indistinguishable from each other. The dashed red lines show the approximations (34) and (36) for $\bar{n} \ll n_{\text{crit}}$ and $\bar{n} \gg n_{\text{crit}}$, respectively. The dot-dashed black line (almost indistinguishable from the lowest blue line) shows the approximation (35). In the approximations we assume large Δ/g , so that $\Gamma_P \approx \Gamma_d$.

Now the initial state is assumed to be $|g, \bar{n}\rangle$, and the jump due to the action of the operator a yields the unnormalized state $a|g, \bar{n}\rangle$, which has a non-zero overlap with the eigenstate $|e, n-2\rangle$, corresponding to the excited state of the qubit. Therefore, the qubit excitation rate is

$$\gamma_E(n) = \kappa |\overline{\langle e, n-2 | a | g, \bar{n} \rangle}|^2, \quad (37)$$

which can be written as [see Eqs. (23)–(25)]

$$\gamma_E(n) = \kappa (\sqrt{n-1} \sin \theta_n \cos \theta_{n-1} - \sqrt{n} \sin \theta_{n-1} \cos \theta_n)^2. \quad (38)$$

Similar to Eq. (30) this rate should be averaged,

$$\gamma_E = \left[\sum_{n=0}^{\infty} P(n) \gamma_E(n) \right] / \sum_{n=0}^{\infty} P(n), \quad (39)$$

over the probability distribution $P(n)$ for the states $|g, \bar{n}\rangle$, for which we will use the coherent-state approximation (31) with mean photon number \bar{n} (a better notation used in the next subsection is \bar{n}_g). The dependence of γ_E on \bar{n} is shown in Fig. 5 by blue solid lines (γ_E is normalized by Γ_P and \bar{n} is normalized by n_{crit}).

Expanding $\gamma_E(n)$ in powers of g/Δ and carrying out the summation (39) produces the series

$$\gamma_E = \kappa \bar{n}^2 \lambda^6 [1 - 5\lambda^2(2\bar{n} + 3) + \lambda^4(69\bar{n}^2 + 276\bar{n} + 159) + \dots], \quad (40)$$

which has the leading-order approximation

$$\gamma_E \approx \frac{\Gamma_d}{16} \left(\frac{\bar{n}}{n_{\text{crit}}} \right)^2 \quad (41)$$

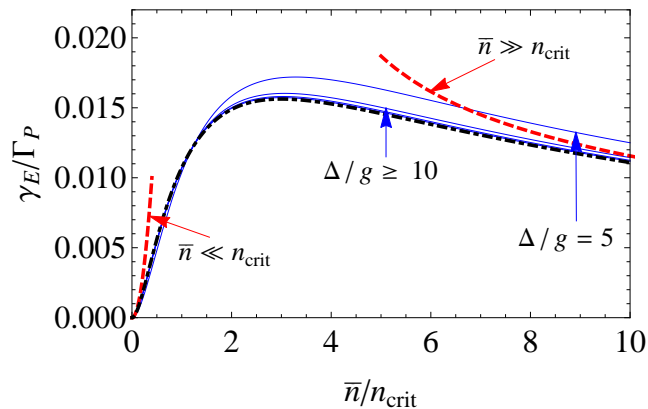


FIG. 5. The qubit excitation rate γ_E [Eq. (39)] normalized by the no-drive relaxation rate Γ_P versus \bar{n}/n_{crit} for several values of Δ/g : 5, 10, 15, and 20 (blue solid lines). The curves for $\Delta/g \geq 15$ are practically indistinguishable from each other. The red dashed lines show the approximations (41) and (42) for $\bar{n} \ll n_{crit}$ and $\bar{n} \gg n_{crit}$, respectively. The dot-dashed black line (barely distinguishable) shows the approximation (43). In the approximations we assume large Δ/g .

at $1 \ll \bar{n} \ll n_{crit}$. This dependence is shown by the left dashed red line in Fig. 5; it works well only when $\bar{n}/n_{crit} \lesssim 0.1$. [The truncated expansion (40) works well until $\bar{n}/n_{crit} \lesssim 0.2$.] Approximating Eq. (38) in the opposite limit, $\bar{n} \gg n_{crit}$, gives

$$\gamma_E \approx \Gamma_d \frac{n_{crit}}{4\bar{n}} \left[1 - 2 \left(\frac{n_{crit}}{\bar{n}} \right)^{1/2} + 3 \left(\frac{n_{crit}}{\bar{n}} \right)^{3/2} \right], \quad (42)$$

which is shown by the right dashed red line in Fig. 5. The approximation for arbitrary \bar{n}/n_{crit} , which assumes $\bar{n} \gg 1$ and $n_{crit} \gtrsim 1$ [derived similar to Eq. (35)] is

$$\gamma_E \approx \frac{\kappa g^2}{4\Delta^2} \left(\frac{1}{1 + \bar{n}/n_{crit}} - \frac{1}{\sqrt{1 + \bar{n}/n_{crit}}} \right)^2. \quad (43)$$

Note that for $\bar{n} \lesssim n_{crit}$ the excitation rate is much smaller than the relaxation rate, $\gamma_E/\Gamma_R \lesssim (\bar{n}/4n_{crit})^2 \ll 1$. However, for $\bar{n} \gg n_{crit}$ the relaxation and excitation rates become identical in the leading order, as follows from Eqs. (36) and (42) (we were not able to reach this regime in numerical simulations discussed in Sec. IV). The dependence $\gamma_E(\bar{n})$ has a maximum (Fig. 5), which for $|\Delta/g| > 3$ occurs at $\bar{n} \approx 3n_{crit}$ [this value follows from Eq. (43)] Even at this maximum the excitation rate is much smaller than the no-drive relaxation rate, $\gamma_E/\Gamma_P < 0.02$, as seen in Fig. 5 [the maximum value which follows from the approximation (43) is $\gamma_E = \Gamma_d/64$].

Our derivation for the relaxation and excitation rates Γ_R and γ_E was based on considering only the “jump” processes caused by the operator a and finding their contribution to transitions between the two ladders of eigenstates in Fig. 2. The remaining (non-unitary) “no jump” evolution and the unitary evolution due to the drive with

amplitude ε also contribute to transitions between the two ladders of eigenstates. However, since these transitions are non-stochastic, the energy shift between the two ladders suppresses the transitions (as expected for a coherent off-resonant process) and prevents the linear-in-time increase of the “wrong” ladder population. This is why these processes are not expected to contribute directly to the relaxation and excitation rates. Nevertheless, the evolution due to the drive and due to the absence of jumps effectively changes the ladders of eigenstates. Thus, at very large \bar{n} our results (29) and (38) for the relaxation and excitation rates are expected to become invalid.

B. Purcell rate with drive: Formal approach

The results of the previous subsection were based on a physical intuition, leading to Eqs. (28) and (37). Here we present a formal derivation of the analytical expression for the Purcell rate with the microwave drive. In the formal approach we need to assume the slightly nonlinear dispersive regime: $|\Delta/g| \gg 1$ and $\bar{n}/n_{crit} \ll 1$. The derivation essentially follows the formalism developed in Ref. [16].

We first transform the master equation (22) to the frame where the JC Hamiltonian is diagonal. While it is simple for wavefunctions [see Eqs. (23) and (24)], it is not so simple for the operator form of the Hamiltonian. This can be done by introducing the transformation \mathbf{D} of the form

$$\mathbf{D} = e^{-\Lambda(N_e)I_-}, \quad (44)$$

where

$$I_{\pm} = \sigma_+ a \pm \sigma_- a^\dagger, \quad N_e = a^\dagger a + |e\rangle\langle e|, \quad (45)$$

N_e is the number operator for total excitations in the system and the function $\Lambda(N_e)$ still has to be determined. After this transformation the master equation reads

$$\dot{\rho}^{\mathbf{D}} = -i[H_I^{\mathbf{D}}, \rho^{\mathbf{D}}] + \kappa \mathcal{D}[a^{\mathbf{D}}]\rho^{\mathbf{D}}, \quad (46)$$

where

$$\rho^{\mathbf{D}} = \mathbf{D}^\dagger \rho \mathbf{D}, \quad a^{\mathbf{D}} = \mathbf{D}^\dagger a \mathbf{D}, \quad H_I^{\mathbf{D}} = \mathbf{D}^\dagger H_I \mathbf{D}, \quad (47)$$

and H_I is given by Eq. (21) (in our notation the wavefunctions are transformed with \mathbf{D}^\dagger rather than with \mathbf{D}). The JC part of the transformed Hamiltonian, $H_{JC}^{\mathbf{D}} = (\Delta/2)\sigma_z^{\mathbf{D}} + gI_+^{\mathbf{D}}$, can then be written as [16]

$$H_{JC}^{\mathbf{D}} = \left[\frac{\Delta}{2} \cos(2\Lambda\sqrt{N_e}) - g\sqrt{N_e} \sin(2\Lambda\sqrt{N_e}) \right] \sigma_z + \left[\frac{\Delta}{2\sqrt{N_e}} \sin(2\Lambda\sqrt{N_e}) + g \cos(2\Lambda\sqrt{N_e}) \right] I_+, \quad (48)$$

where $\Lambda = \Lambda(N_e)$. Note that here we treated the operator N_e in the square root as a c -number. This is possible

because N_e is a positive operator and its square root is defined via taking the square root of the eigenvalues in the diagonalizing basis. Also note that Λ commutes with $\sqrt{N_e}$, and that the $\sqrt{N_e}$ in denominator is canceled when the sine function is expanded.

Since we want to diagonalize the JC Hamiltonian, we need to eliminate the second line of Eq. (48) by zeroing the coefficient of I_+ , which can be done by choosing

$$\Lambda = -\frac{1}{2\sqrt{N_e}} \arctan\left(\sqrt{4\lambda^2 N_e}\right). \quad (49)$$

Then the transformed JC Hamiltonian is only the first line of Eq. (48), which using Eq. (49) can be written as

$$H_{JC}^D = \frac{\Delta}{2} \sqrt{1 + 4\lambda^2 N_e} \sigma_z = \frac{\Delta}{2} \sqrt{1 + N_e/n_{\text{crit}}} \sigma_z. \quad (50)$$

This is exactly the desired Hamiltonian for the qubit-resonator system in the eigenbasis – see Eq. (26).

Next, we find explicit form of the \mathbf{D} -transformed annihilation operator a , which enters the drive Hamiltonian and the Lindblad term of the master equation (46). Calculating $\mathbf{D}^\dagger a \mathbf{D}$ by expanding the exponent in the definition of \mathbf{D} , we obtain

$$a^{\mathbf{D}} = a - [a, \Lambda I_-] + \frac{1}{2!} [[a, \Lambda I_-], \Lambda I_-] + \dots \quad (51)$$

Then by expanding $\Lambda(N_e)$ [using Eq. (49)] in powers of $\sqrt{4\lambda^2 N_e}$ with the assumption that $\sqrt{4\lambda^2 N_e} < 1$ (i.e. $N_e < n_{\text{crit}}$) and explicitly computing the resulting commutation relations, we obtain after a lengthy algebra the following expression,

$$a^{\mathbf{D}} = a_1^{\mathbf{D}} + a_2^{\mathbf{D}} + a_3^{\mathbf{D}}, \quad (52)$$

with

$$a_1^{\mathbf{D}} = \left\{ 1 + \frac{\lambda^2}{2} \sigma_z - \frac{\lambda^4}{8} [12(\hat{n} + 1)\sigma_z + 1] + \lambda^6 \left[\left(5\hat{n}^2 + 10\hat{n} + \frac{73}{16} \right) \sigma_z + \frac{\hat{n} + 1}{4} \right] + \dots \right\} a, \quad (53)$$

$$a_2^{\mathbf{D}} = \lambda \left\{ 1 - \frac{3}{2} \lambda^2 (2\hat{n} + 1) + \lambda^4 \left(11\hat{n}^2 + 11\hat{n} + \frac{31}{8} \right) - \lambda^6 \left(42\hat{n}^3 + 63\hat{n}^2 + \frac{355}{8} \hat{n} + \frac{187}{16} \right) + \dots \right\} \sigma_-, \quad (54)$$

$$a_3^{\mathbf{D}} = \lambda^3 \left\{ 1 - \frac{5\lambda^2}{2} (2\hat{n} + 3) + \lambda^4 \left(22\hat{n}^2 + 66\hat{n} + \frac{411}{8} \right) + \dots \right\} a^2 \sigma_+, \quad (55)$$

where $\hat{n} = a^\dagger a$ is the photon number operator. Note that in the transformed frame the field operator $a^{\mathbf{D}}$ acquires a qubit part ($a_2^{\mathbf{D}}$ is proportional to σ_- and $a_3^{\mathbf{D}}$ is proportional to $a^2 \sigma_+$). Equation (52) has the following interpretation. Each term describes an “annihilation” process, which reduces the number of excitations by 1. The first term $a_1^{\mathbf{D}}$ (proportional to a) describes annihilation of a photon in the eigenbasis, which is modified due to the presence of the qubit. The second term $a_2^{\mathbf{D}}$,

which describes qubit relaxation, also reduces the number of excitations by 1. Thus the photon annihilation process is partly converted into qubit relaxation: this second term eventually leads to the Purcell relaxation. The last term $a_3^{\mathbf{D}}$, which describes annihilation of two photons and qubit excitation, also reduces the number of excitations by 1. This process leads to qubit excitation as a result of leakage of photons through the resonator. There are no more groups of terms because qubit cannot absorb or emit more than one excitation, and thus there are no more processes decreasing the total number of excitations by 1.

It is interesting to relate the terms in Eq. (52) with the matrix elements of a in the eigenbasis, considered in the previous subsection. Since $a^{\mathbf{D}}$ is essentially the operator a in the eigenbasis, we would expect that $a^{\mathbf{D}}$ sandwiched between two bare states should be equal to the operator a sandwiched between the corresponding eigenstates so that

$$\overline{\langle e, n-1 | a | e, n \rangle} = \langle e, n-1 | a_1^{\mathbf{D}} | e, n \rangle, \quad (56)$$

$$\overline{\langle g, n | a | e, n \rangle} = \langle g, n | a_2^{\mathbf{D}} | e, n \rangle, \quad (57)$$

$$\overline{\langle e, n-2 | a | g, n \rangle} = \langle e, n-2 | a_3^{\mathbf{D}} | g, n \rangle. \quad (58)$$

We have checked these relations explicitly using the truncated expansions (53)–(55) and corresponding expansions of the eigenstates (23)–(25). These relations give us an insight why the formal-approach results which we will obtain later are essentially equivalent to the results of the simple approach.

The next step in the derivation is to use the polaron-type transformation described below.

Polaron-type transformation

We expect that in the eigenbasis the quasi-stationary state is close to a coherent state within the subspace of “excited” eigenstates (right ladder of red dashed lines in Fig. 2) and also close to a (possibly different) coherent state within the subspace of “ground state” eigenstates (left ladder of dashed lines). Therefore, it is natural to apply displacement transformations within these (eigen) ladders, which transform the coherent states to the lowest levels in the ladders. In this way the case with the microwave drive should, to a considerable extent, be reduced to the case without the microwave drive, thus simplifying the analysis.

Formally, we apply the polaron-type [29] transformation \mathbf{P} to the master equation (46), so that the density operator transforms as $\rho^{\mathbf{D}\mathbf{P}} = \mathbf{P}^\dagger \rho^{\mathbf{D}} \mathbf{P}$ with

$$\mathbf{P} = |e\rangle \langle e| D(\alpha_e) + |g\rangle \langle g| D(\alpha_g), \quad (59)$$

where $D(\alpha)$ is the usual displacement operator and $\alpha_{e(g)}$ are resonator field amplitudes corresponding to the qubit state $|e\rangle$ or $|g\rangle$. Note that Eq. (59) formally uses the bare states, but the conversion between bare states and

eigenstates is already performed by the transformation \mathbf{D} . Also note that we apply \mathbf{P}^\dagger (not \mathbf{P}) to the wavefunctions, so this is a displacement by $-\alpha_{e(g)}$. So far the amplitudes $\alpha_e(t)$ and $\alpha_g(t)$ are arbitrary and in general time-dependent. The master equation after the polaron-type transformation becomes

$$\begin{aligned} \dot{\rho}^{\mathbf{DP}} = & -i[H_{JC}^{\mathbf{DP}} + \varepsilon(a^{\mathbf{DP}} + a^{\dagger\mathbf{DP}}), \rho^{\mathbf{DP}}] + \kappa\mathcal{D}[a^{\mathbf{DP}}]\rho^{\mathbf{DP}} \\ & + i[\text{Im}(T_\alpha \dot{T}_\alpha^*), \rho^{\mathbf{DP}}] + [a\dot{T}_\alpha^* - a^\dagger\dot{T}_\alpha, \rho^{\mathbf{DP}}], \end{aligned} \quad (60)$$

where $T_\alpha = \alpha_e|e\rangle\langle e| + \alpha_g|g\rangle\langle g|$ and the second line in this equation is due to time-dependence of $\alpha_e(t)$ and $\alpha_g(t)$. The explicit form of the master equation (60) is very lengthy and we do not present it here. Its perturbative form can be obtained by first expanding the Hamiltonian $H_{JC}^{\mathbf{D}}$ in powers of N_e/n_{crit} [see Eq. (50)] and then applying the \mathbf{P} -transformation to the field and qubit operators,

$$\mathbf{P}^\dagger a \mathbf{P} = a + T_\alpha, \quad (61)$$

$$\sigma_z^{\mathbf{P}} = \sigma_z, \quad \mathbf{P}^\dagger \sigma_- \mathbf{P} = D(\alpha_g)^\dagger D(\alpha_e) \sigma_-, \quad (62)$$

while the transformation of higher-order terms for field operators can be obtained using sequential application of (61), for example,

$$\mathbf{P}^\dagger \hat{n} \mathbf{P} = \hat{n} + aT_\alpha^* + a^\dagger T_\alpha + |T_\alpha|^2, \quad (63)$$

$$\begin{aligned} \mathbf{P}^\dagger \hat{n}^2 \mathbf{P} = & [(1 + 2|T_\alpha|^2)T_\alpha^* a + a^2 T_\alpha^{*2} + 2\hat{n} a T_\alpha^* + \text{H.c.}] \\ & + |T_\alpha|^2 (4\hat{n} + 1) + \hat{n}^2 + |T_\alpha|^4. \end{aligned} \quad (64)$$

Now we want to find “good” values of α_e and α_g , which correspond to the quasi-stationary state. This can be done using the following trick. Let us impose the condition that the total coefficient for the operator a^\dagger in the transformed master equation (60) is zero (then the coefficient for a also vanishes automatically). This would correspond to the situation without drive (in the effective frame), and then because of the relaxation due to κ , the lowest state within each ladder will be eventually reached, independent of the initial state. [This will not be exact because of non-zero terms $(a^\dagger)^2$, $(a^\dagger)^3$, etc., but this is good as an approximation.] Imposing this condition and keeping terms up to λ^4 , we obtain equations

$$\begin{aligned} \dot{\alpha}_j(t) \approx & -\frac{\kappa}{2} [1 \pm \lambda^2(1 - 6\lambda^2\bar{n}_j)] \alpha_j \\ & + i\chi\{\lambda^2 \mp [1 - 2\lambda^2(\bar{n}_j + 1)]\} \alpha_j \\ & - i\varepsilon \left\{ 1 - \frac{\lambda^4}{8} \pm \frac{\lambda^2}{2} [1 - 3\lambda^2(2\bar{n}_j + 1)] \right\}, \end{aligned} \quad (65)$$

with the top sign for $j = e$ and the bottom sign for $j = g$; here $\bar{n}_j = |\alpha_j|^2$ is the corresponding mean photon number and $\chi = g^2/\Delta$ is the resonator frequency shift in the strong dispersive regime ($\lambda \ll 1$, $\bar{n}_j \ll n_{\text{crit}}$). In Eq. (65) the term proportional to κ is a contribution from the Lindblad master equation, the term proportional to χ is a contribution from JC Hamiltonian, and the last term is due to the microwave drive. It is easy to see that Eq. (65) is essentially the equation for classical field

amplitudes $\alpha_{e(g)}(t)$, as expected. The stationary solution of this equation, $\dot{\alpha}_j(t) = 0$, gives the steady-state values α_e and α_g , which are then substituted into the master equation (60).

With these “good” values of α_e and α_g , we expect a significant population of only two states in the \mathbf{DP} -transformed frame: $|e, 0\rangle$ and $|g, 0\rangle$. We also expect that these populations, $\rho_{e0,e0}^{\mathbf{DP}}$ and $\rho_{g0,g0}^{\mathbf{DP}}$, are close to the total occupation of the right and left ladders of eigenstates in Fig. 2. Therefore the transition rates between the states $|e, 0\rangle$ and $|g, 0\rangle$ in the \mathbf{DP} -transformed frame should give the relaxation and excitation rates for the qubit; these rates can now be found from Eq. (60). The expansion form of the equation for $\rho_{e0,e0}^{\mathbf{DP}}$ is very lengthy and we do not show it here, but if we keep only the terms with $\rho_{e0,e0}^{\mathbf{DP}}$ and $\rho_{g0,g0}^{\mathbf{DP}}$, we then obtain

$$\dot{\rho}_{e0,e0}^{\mathbf{DP}} \approx -\Gamma_R \rho_{e0,e0}^{\mathbf{DP}} + \gamma_E \rho_{g0,g0}^{\mathbf{DP}}, \quad (66)$$

where (to order λ^8) we find

$$\begin{aligned} \Gamma_R = & \kappa\lambda^2 [1 - 3\lambda^2(2\bar{n}_e + 1) + \lambda^4(31\bar{n}_e^2 + 62\bar{n}_e + 10) \\ & - \lambda^6(150\bar{n}_e^3 + 675\bar{n}_e^2 + 520\bar{n}_e + 35)], \end{aligned} \quad (67)$$

and (to order λ^{10})

$$\gamma_E = \kappa\bar{n}_g^2\lambda^6 [1 - 5\lambda^2(2\bar{n}_g + 3) + \lambda^4(69\bar{n}_g^2 + 276\bar{n}_g + 159)]. \quad (68)$$

These results for the relaxation and excitation rates Γ_R and γ_E are in exact agreement with Eqs. (33) and (40), obtained using the simple intuitive approach. Note however that since our formal derivation was based on the expansion in λ , it can be used only for relatively small values of the nonlinearity parameter $\bar{n}_{e(g)}/n_{\text{crit}}$ (see, e.g., the green dashed line in Fig. 3), in contrast to the simple approach.

Thus the results (67) and (68) of the formal approach confirm that the Purcell relaxation rate decreases with increasing strength of the microwave drive, and there exists a relatively weak qubit excitation due to resonator damping. The results of the formal approach are essentially an extension of the previous work [16], where only the leading order was considered, and hence the photon-number-dependent Purcell rate and the excitation rate were not obtained.

C. Physical interpretation

We do not have a complete physical interpretation of the Purcell relaxation suppression due to additional photons induced by the microwave drive, so we may say that this is just the mathematical property of the matrix element $\langle g, n|a|e, n\rangle$ [see Eq. (28)], which decreases with n . However, we have a crude physical interpretation. The idea is that the additional drive changes the effective qubit frequency due to the ac (dynamic) Stark shift,

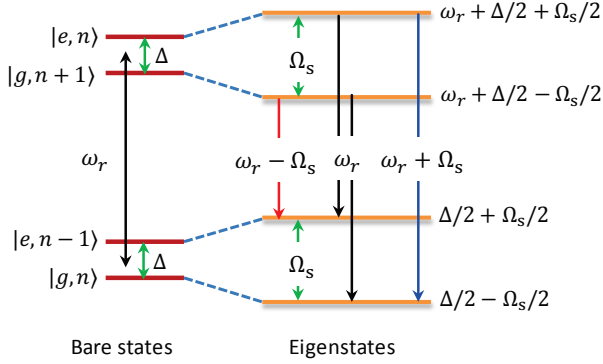


FIG. 6. Four neighboring levels of the Jaynes-Cummings ladder of Fig. 2, redrawn in a slightly different way. The shown energy is relative to the energy of the state $|g, n\rangle$. Assuming $n \approx \bar{n} \gg 1$, the level splitting in both pairs of eigenstates is approximately $|\Omega_S| = \sqrt{\Delta^2 + 4g^2\bar{n}}$. The level splitting increases with \bar{n} . There are four possible transitions marked by down arrows; two of them have frequencies almost coinciding with ω_r (neglecting the dispersive shift), and two of them are at frequencies $\omega_r \pm \Omega_S$. These transitions can be thought of as the Mollow triplet [30] at non-zero detuning.

which increases the detuning $|\Delta|$. Then if we use the formula for the single-excitation Purcell rate [Eqs. (16) or (17)], we find the suppression of the rate with increasing mean photon number \bar{n} .

More quantitatively, the effective detuning with $\bar{n} \gg 1$ photons is the level splitting between the eigenstates of the JC ladder (see Figs. 2 and 6),

$$\Omega_S = \sqrt{\Delta^2 + 4\bar{n}g^2} \operatorname{sgn}(\Delta) = \Delta\sqrt{1 + \bar{n}/n_{\text{crit}}}. \quad (69)$$

(Note that the resonator frequency changes by less than $g^2/\Delta = \Delta/4n_{\text{crit}}$, so the change of effective detuning is mostly due to the qubit frequency change.) In the regime $\bar{n} \ll n_{\text{crit}}$, this gives the effective detuning $\Delta(1 + \bar{n}/2n_{\text{crit}})$. Therefore, if we use the dispersive single-excitation formula $\Gamma_d = \kappa g^2/\Delta^2$ [Eq. (16)] with increased $|\Delta|$, we would expect the Purcell rate suppression as $\Gamma_R \approx \Gamma_d(1 - \bar{n}/n_{\text{crit}})$, which is different from the actual result [Eq. (34)] by the missing factor 3/2. The additional suppression could in principle be explained by the change of effective κ (due to decreasing overlap); however, we did not find a reasonable quantitative explanation of this kind. Besides the difficulty with quantitative explanation of the suppression, a natural question is why we can still use the no-drive formula (16), essentially mixing the linear and nonlinear approaches to the dynamics. Thus we cannot call the physical interpretation based on the ac Stark shift a perfect interpretation.

Note that it is also possible to discuss the reduction of the qubit relaxation rate and appearance of the nonzero excitation rate in terms of the Mollow triplet physics [30] at non-zero detuning Δ (Fig. 6). In our case the triplet is transformed into a quadruplet (neglecting the “fine structure” due to n -dependence of the transition frequencies).

The two central “peaks” correspond to the qubit-state-dependent resonator frequency $\omega_r \pm g^2/\Omega_S$; the difference between them is used for the qubit readout [7, 23–25] (the quadruplet becomes a triplet if the dispersive shift $\pm g^2/\Omega_S$ is neglected, as in Fig. 6). The two side peaks correspond to the qubit relaxation and excitation (Fig. 6). In the case of relaxation the qubit emits the photon with frequency approximately $\omega_r + \Omega_S$. In the case of excitation the qubit absorbs this energy, which is taken from two photons in the resonator, so that the photon emitted into the transmission line has frequency $\omega_r - \Omega_S$. With increasing drive (increasing \bar{n}) the side peaks move further away from the central peaks (ac Stark shift). As discussed above, this leads to the suppression of the relaxation rate Γ_R (at least qualitatively). The excitation rate γ_E first increases with increasing \bar{n} , as expected for a two-photon process, but eventually the suppression due to increasing detuning becomes the dominating effect, and γ_E starts to decrease.

IV. NUMERICAL RESULTS

Besides developing the analytical approaches discussed in the previous section, we have also solved the full master equation (22) for the qubit-resonator system numerically and thus computed the qubit relaxation and excitation rates. In this section we present the numerical results and compare them with analytical results.

A. Qubit relaxation rate

Since we do not consider intrinsic qubit relaxation as well as dressed dephasing (a process which converts pure dephasing into photon-number-dependent qubit relaxation), the decay rate obtained from the numerical solution is only due to the Purcell effect. To calculate the relaxation rate we start with an initial state that is the coherent-state superposition of the eigenstates corresponding to the excited state of the qubit [14] (right ladder of red dashed lines in Fig. 2),

$$|\psi_{\text{in}}\rangle = e^{-|\alpha_{\text{in}}|^2/2} \sum_{n=0}^{\infty} \frac{\alpha_{\text{in}}^n}{\sqrt{n!}} |e, n\rangle, \quad (70)$$

where α_{in} is the initial amplitude of the resonator field. For α_{in} we use the value $\alpha_{\text{in}} = -i\varepsilon/[i(g^2/\Delta + \omega_r - \omega_d) + \kappa/2]$, obtained classically by assuming that the resonator frequency is increased by g^2/Δ due to the qubit in the excited state (recall that the driving frequency ω_d is exactly ω_r). The corresponding mean photon number is $\bar{n}_{\text{in}} = |\alpha_{\text{in}}|^2 = 4|\varepsilon|^2/[4(g^2/\Delta + \omega_r - \omega_d)^2 + \kappa^2]$. However, this initial value of α_{in} is good only in the linear regime when $\bar{n} \ll n_{\text{crit}}$. In the non-linear regime the effective resonator frequency becomes (see Fig. 2) $\omega_r + \Delta(\sqrt{1 + \bar{n}/n_{\text{crit}}} - \sqrt{1 + (\bar{n} - 1)/n_{\text{crit}}}) \approx \omega_r + g^2/\Omega_S$,

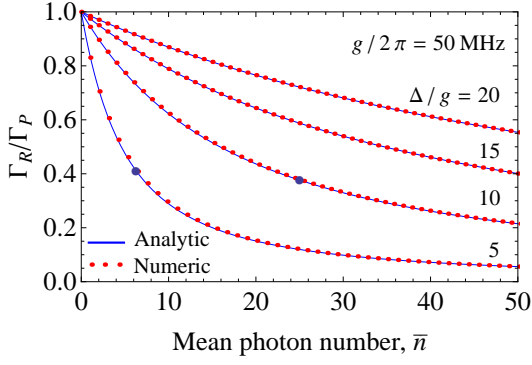


FIG. 7. Normalized Purcell rate Γ_R/Γ_P vs the mean photon number for $\kappa = g = 2\pi \times 50$ MHz and several values of detuning: $\Delta/g = 5, 10, 15,$ and 20 . The red dots show the results obtained numerically, blue solid lines are calculated using Eq. (30). The large blue dots indicate the critical photon number n_{crit} .

where the level splitting Ω_S is given by Eq. (69). Therefore the quasi-steady state is expected to have $\alpha_e \approx -i\varepsilon/[i(g^2/\Omega_S + \omega_r - \omega_d) + \kappa/2]$ and the corresponding mean photon number is expected to be

$$\bar{n} = \frac{|\varepsilon|^2}{(g^2/\sqrt{\Delta^2 + 4g^2\bar{n}} + \omega_r - \omega_d)^2 + (\kappa/2)^2}. \quad (71)$$

This equation allows easy calculation of ε for a desired \bar{n} . Note that for the qubit in the ground state, the frequency shift g^2/Ω_S is replaced with $-g^2/\Omega_S$. However, since we use $\omega_d = \omega_r$, the mean photon number \bar{n} given by Eq. (71) does not change. Therefore, \bar{n} is not affected by the Purcell relaxation. Also note that Eq. (71) does not show bistability when $\omega_d = \omega_r$, though the bistability occurs for a range of detuning $\omega_d - \omega_r \neq 0$ if $\kappa < 4g^4\bar{n}/\Omega_S^3$. In simulations we first find ε for a desired \bar{n} analytically, but then calculate the actual \bar{n} numerically. We have checked that Eq. (71) works quite well for the parameters we used, but still not perfectly.

We use the bare basis to compute the evolution using the master equation (22), but then convert the results into the eigenbasis; in particular, we monitor the population of the excited qubit state in the eigenbasis,

$$\bar{\rho}_{ee}(t) = \sum_n \text{Tr}[\rho(t) |e, n\rangle \langle e, n|]. \quad (72)$$

The use of the initial condition (70) allows us to mostly avoid initial oscillations of $\bar{\rho}_{ee}(t)$ (decaying on the timescale $\sim \kappa^{-1}$), so that the decay of $\bar{\rho}_{ee}$ is smooth in time, and therefore the Purcell rate Γ_R can be relatively easily defined numerically as the slope of the dependence $-\ln[\bar{\rho}_{ee}(t)]$, which is close to a straight line for a sufficiently long duration. Note that because of a non-zero excitation rate, the dependence $\bar{\rho}_{ee}(t)$ eventually saturates at a non-zero value; therefore it is necessary to restrict the time duration, making sure that $\bar{\rho}_{ee}$ remains much larger than the saturation value.

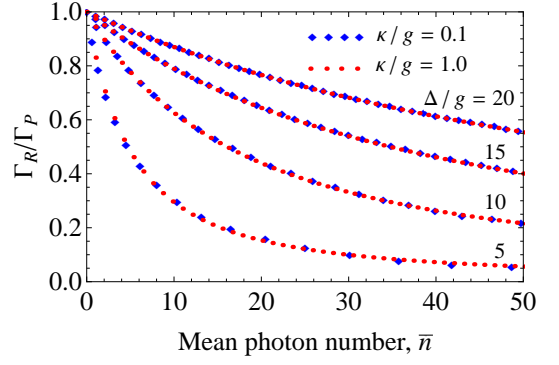


FIG. 8. Numerical results for the normalized Purcell rate Γ_R/Γ_P as a function of \bar{n} for $\kappa/g = 0.1$ (blue diamonds) and $\kappa/g = 1$ (red dots); the detuning parameter is $\Delta/g = 5, 10, 15,$ and 20 (as in Fig. 7).

Red dots in Fig. 7 show the numerically calculated Purcell rate Γ_R [normalized by the no-drive value Γ_P given by Eq. (17)] as a function of the steady-state mean photon number \bar{n} in the resonator, for $\kappa = g$ and several values of Δ/g (the calculations have been done for $g/2\pi = 50$ MHz, but the results do not depend on g because of the linear overall scaling). The solid lines show the approximate analytical result, obtained in the simple approach, Eq. (30). We see a very good agreement between the analytics and numerics. It is important that the Purcell rate continues to decrease when \bar{n} is significantly larger than n_{crit} , and agreement with analytics is still very good in this regime. The numerical results confirm that the Purcell rate suppression can be more than an order of magnitude.

The analytics [Eqs. (28)–(30)] predict that the Purcell rate Γ_R scales linearly with κ (keeping the same \bar{n}). In Fig. 8 we check this scaling numerically by comparing the results for $\kappa/g = 1$ (red dots, same as in Fig. 7) and for $\kappa/g = 0.1$ (blue diamonds). (Note that $\kappa/g = 0.1$ and even lower values are typical in circuit QED experiments). We see that the numerical results confirm, at least in this regime, the simple scaling of Γ_R with κ (so that Γ_R/Γ_P does not depend on κ) for the same value of \bar{n} . Note however that decreasing κ assumes decreasing drive amplitude ε to keep \bar{n} fixed.

B. Qubit excitation rate

We have also calculated numerically the qubit excitation rate due to the resonator decay. For that we start with the initial state, which is the superposition of the eigenstates corresponding to the ground state of the qubit:

$$|\psi_{\text{in}}\rangle = e^{-|\alpha_{\text{in}}|^2/2} \sum_{n=0}^{\infty} \frac{\alpha_{\text{in}}^n}{\sqrt{n!}} |g, n\rangle, \quad (73)$$

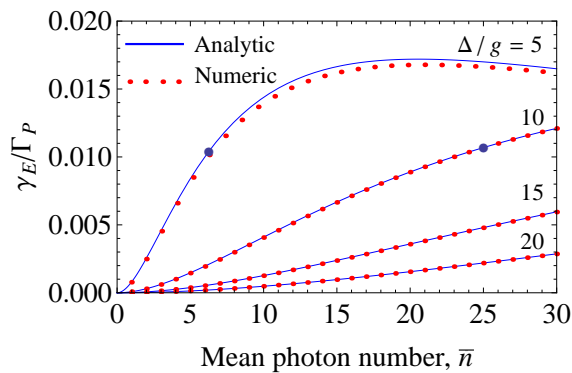


FIG. 9. The qubit excitation rate γ_E (normalized by the no-drive relaxation rate Γ_P) as a function of \bar{n} for $\kappa = g$ (we used $g/2\pi = 50$ MHz) and several values of detuning, $\Delta/g=5, 10, 15,$ and 20 . The red dots show the numerical results, the blue solid lines are obtained analytically using Eq. (39). The large blue dots indicate n_{crit} .

where α_{in} now corresponds to the ground state of the qubit, $\alpha_{\text{in}} = -i\varepsilon/[i(-g^2/\Delta + \omega_r - \omega_d) + \kappa/2]$ or in a better approximation $\alpha_g = -i\varepsilon/[i(-g^2/\Omega_S + \omega_r - \omega_d) + \kappa/2]$. Since we use $\omega_d = \omega_r$, only the phase of α_{in} is different from what was used in Eq. (70), while \bar{n}_{in} is still the same. Note that the initial value α_{in} is not very important because the system converges to the quasi-steady-state value of α within few resonator lifetimes κ^{-1} . Similar to what was discussed in the previous subsection, we calculate the quasi-steady-state value of \bar{n} numerically.

Following the same procedure as for computing the qubit relaxation rate, we calculate the qubit excitation rate γ_E . The only difference is that now we monitor the decrease of $\bar{p}_{gg}(t) = 1 - \bar{p}_{ee}(t)$, and the qubit excitation rate γ_E is defined numerically as the negative slope of $\ln[\bar{p}_{gg}(t)]$ during a time range when this dependence is linear (this time range should be much shorter than Γ_R^{-1}).

Figure 9 shows the excitation rate γ_E normalized by the no-drive Purcell rate Γ_P [Eq. (17)], as a function of the mean photon number \bar{n} . The excitation rate is quite weak and first increases with the strength of the microwave field. The rate also depends on the detuning: the smaller the detuning, the larger the excitation rate becomes. The rate calculated numerically agrees well with the analytical result given by Eqs. (39). As discussed in Sec. IIIA, the dependence $\gamma_E(\bar{n})$ should reach maximum at $\bar{n} \approx 3n_{\text{crit}}$ (when $\Delta/g > 3$). Figure 9 confirms this behavior for $\Delta/g = 5$. Even at the maximum, the value of γ_E remains much smaller than Γ_P (over 50 times), and at this point it is ~ 8 times smaller than Γ_R .

V. CONCLUSION

We have analyzed the Purcell relaxation rate of a superconducting qubit coupled to a leaking microwave resonator, which is pumped on-resonance by an external mi-

crowave drive. The main result is that the Purcell rate Γ_R is suppressed due to the presence of photons in the resonator, with the strong suppression obtained in the nonlinear regime. The presence of photons in the resonator also leads to qubit excitation, but the excitation rate γ_E is always much smaller than the no-drive Purcell relaxation rate Γ_P . We have derived approximate analytical formulas for the relaxation and excitation rates [e.g., Eqs. (29), (35), (38), and (43)], which agree well with the numerical results.

In this work we assumed a time-independent drive amplitude ε . It is rather simple to introduce a time-dependent drive $\varepsilon(t)$ to describe experiments with short measurement time, as long as the dynamics is sufficiently adiabatic (which is almost always the case in experiments – see Ref. [14]). Using the simple intuitive approach (Sec. IIIA), we first solve the classical equations for the field with account of nonlinearity to find $\bar{n}(t)$ and then obtain the corresponding time-dependent Purcell rate $\Gamma_R(t)$ and the excitation rate $\gamma_E(t)$. In the formal perturbative approach (Sec. IIIB) the evolution of the field can be taken into account automatically via Eq. (65).

To experimentally observe the Purcell rate suppression with increasing microwave drive predicted in this work, it is important to make sure that other mechanisms do not increase the qubit relaxation rate faster than the obtained suppression. One such mechanism for superconducting qubits is the dressed dephasing [15–17], which increases the relaxation rate as $\Gamma_{\downarrow, \text{dd}} \simeq \gamma_\varphi \bar{n}/2n_{\text{crit}}$, where γ_φ is the pure dephasing rate (this formula assumes a similar noise spectrum at the qubit frequency ω_q and at low frequency). This increase is weaker than the first-order Purcell rate suppression $-3\bar{n}\Gamma_P/2n_{\text{crit}}$ [see Eq. (33)] if the no-drive Purcell rate $\Gamma_P \approx \Gamma_d = \kappa g^2/\Delta^2$ exceeds the pure dephasing, $\Gamma_P > \gamma_\varphi/3$. Therefore, to observe the Purcell rate suppression experimentally, it may be necessary to deliberately increase the Purcell rate by decreasing the detuning Δ and/or increasing the resonator damping rate κ and coupling g . Note an indication of possible Purcell rate suppression in a recent experiment – see Fig. S7 in Ref. [24].

In this paper we treated the qubit as a two-level system. In reality, most of present-day superconducting qubits are essentially only slightly nonlinear oscillators, with almost equidistant energy spectrum. The anharmonicity $\mathcal{A} = 2E_{|e\rangle} - E_{|g\rangle} - E_{|f\rangle}$ (with $|f\rangle$ being the next excited level) is typically much smaller than the qubit frequency ($\mathcal{A}/\omega_q \simeq 0.03 - 0.05$) and only a few times larger than the coupling $|g|$. The presence of the level $|f\rangle$ does not affect the no-drive Purcell rate Γ_P ; however, it affects the qubit relaxation and excitation rates when the microwave drive is applied. The analysis of this effect is beyond the scope of this paper, but we have done preliminary calculations based on the natural extension of Eqs. (28) and (37), assuming that they are still applicable. These calculations show that the Purcell rate is still suppressed with increasing photon number \bar{n} in the typical regime ($\mathcal{A} > 0, \omega_q < \omega_r$), though the suppression is

weaker than in the two-level model. We have also found that the suppression can still be crudely (not quantitatively) described as being due to the ac Stark shift of the qubit frequency.

In the slightly nonlinear regime the repulsion of the level $|e, n\rangle$ from the level $|f, n-1\rangle$ (which is added to the repulsion between the levels $|e, n\rangle$ and $|g, n+1\rangle$) leads to the effective detuning $\Delta_{\text{eff}} = \Delta + 2(n+1)g^2/\Delta - n(\sqrt{2}g)^2/(\Delta - \mathcal{A})$, where $\sqrt{2}g$ is the approximate coupling constant for the transitions between $|e\rangle$ and $|f\rangle$. This can be rewritten as

$$\Delta_{\text{eff}} = \Delta \left(1 + \frac{n}{2\tilde{n}_{\text{crit}}} \right), \quad \tilde{n}_{\text{crit}} = \frac{\Delta^2}{4g^2} \frac{\mathcal{A} - \Delta}{\mathcal{A}}, \quad (74)$$

where \tilde{n}_{crit} is the appropriately redefined critical photon number (27), which takes into account the third level, and we assumed $1 \ll n \ll n_{\text{crit}} \times \min[1, (\Delta - \mathcal{A})^2/2\Delta^2]$ (so that both level repulsions are in almost linear regimes). Note that the effective qubit-state-dependent change of the resonator frequency (which is used for the qubit measurement) is governed by the similar factor, $\omega_{r,(e)}^{\text{eff}} - \omega_{r,(g)}^{\text{eff}} = d\Delta_{\text{eff}}/dn = \Delta/(2\tilde{n}_{\text{crit}})$ for the same range of n . Now crudely estimating the Purcell rate as $\Gamma_R \simeq \kappa(g/\Delta_{\text{eff}})^2$, we obtain the crude estimate of the Purcell rate suppression as $\Gamma_R/\Gamma_P \simeq 1 - n/\tilde{n}_{\text{crit}}$ when $1 \ll n \ll n_{\text{crit}} \times \min[1, (\Delta - \mathcal{A})^2/2\Delta^2]$. This has the same form as Eq. (34), with n_{crit} replaced by \tilde{n}_{crit} and with absent factor $3/2$, which cannot be obtained in this crude derivation (preliminary numerical results indicate that this factor, describing the difference between

the numerical suppression and the Stark-shift model becomes closer to 1). Note that for positive \mathcal{A} and negative Δ (i.e. $\omega_q < \omega_r$, which is the more typical situation for transmon qubits) the effective critical photon number (74) is increased, $\tilde{n}_{\text{crit}} > n_{\text{crit}}$ (strongly increased if $-\Delta \gg \mathcal{A}$), and therefore the Purcell rate suppression is weaker than in the two-level model. (For large ratios $-\Delta/\mathcal{A}$ preliminary numerical results indicate that the suppression is not as weak as follows from strongly increased \tilde{n}_{crit} .) A more complete analysis of the effect of the third and higher levels on the Purcell rate (including the numerical simulations as in Sec. IV) is the subject of a further research.

ACKNOWLEDGMENTS

We thank Howard Carmichael, Klaus Mølmer, Daniel Sank, and John Martinis for useful discussions. We also thank Justin Dressel for a critical reading of the manuscript. This research was funded by the Office of the Director of National Intelligence (ODNI), Intelligence Advanced Research Projects Activity (IARPA), through the Army Research Office Grants No. W911NF-10-1-0334 and No. W911NF-10-1-0324. All statements of fact, opinion or conclusions contained herein are those of the authors and should not be construed as representing the official views or policies of IARPA, the ODNI, or the U.S. Government. We also acknowledge support from the ARO MURI Grant No. W911NF-11-1-0268.

-
- [1] E. M. Purcell, Phys. Rev. **69**, 681 (1946).
 [2] P. Goy, J. M. Raimond, M. Gross, and S. Haroche, Phys. Rev. Lett. **50**, 1903 (1983).
 [3] D. Kleppner, Phys. Rev. Lett. **47**, 233 (1983).
 [4] R. G. Hulet, R. S. Hilfer, and D. Kleppner, Phys. Rev. Lett. **55**, 2137 (1985).
 [5] W. Jhe, A. Anderson, E. A. Hinds, D. Meschede, L. Moi, and S. Haroche, Phys. Rev. Lett. **58**, 666 (1987).
 [6] D. Esteve, M. H. Devoret, and J. M. Martinis, Phys. Rev. B **34**, 158 (1986).
 [7] A. Blais, R. S. Huang, A. Wallraff, S. M. Girvin, and R. J. Schoelkopf, Phys. Rev. A **69**, 062320 (2004).
 [8] A. Wallraff, D. I. Schuster, A. Blais, L. Frunzio, R. S. Huang, J. Majer, S. Kumar, S. M. Girvin, and R. J. Schoelkopf, Nature **431**, 162 (2004).
 [9] A. A. Houck, J. A. Schreier, B. R. Johnson, J. M. Chow, Jens Koch, J. M. Gambetta, D. I. Schuster, L. Frunzio, M. H. Devoret, S. M. Girvin, and R. J. Schoelkopf, Phys. Rev. Lett. **101**, 080502 (2008).
 [10] M. D. Reed, B. R. Johnson, A. A. Houck, L. DiCarlo, J. M. Chow, D. I. Schuster, L. Frunzio, and R. J. Schoelkopf, Appl. Phys. Lett. **96**, 203110 (2010).
 [11] E. Jeffrey, D. Sank, J. Y. Mutus, T. C. White, J. Kelly, R. Barends, Y. Chen, Z. Chen, B. Chiaro, A. Dunsworth, A. Megrant, P. J. J. O'Malley, C. Neill, P. Roushan, A. Vainsencher, J. Wenner, A. N. Cleland, and J. M. Martinis, arXiv:1401.0257.
 [12] J. M. Gambetta, A. A. Houck, and A. Blais, Phys. Rev. Lett. **106**, 030502 (2011).
 [13] Y. Yin, Y. Chen, D. Sank, P. J. J. O'Malley, T. C. White, R. Barends, J. Kelly, E. Lucero, M. Mariantoni, A. Megrant, C. Neill, A. Vainsencher, J. Wenner, A. N. Korotkov, A. N. Cleland, and J. M. Martinis, Phys. Rev. Lett. **110**, 107001 (2013).
 [14] E. A. Sete, A. Galiatdinov, E. Mlinar, J. M. Martinis, and A. N. Korotkov, Phys. Rev. Lett. **110**, 210501 (2013).
 [15] M. Boissonneault, J. M. Gambetta, and A. Blais, Phys. Rev. A **77**, 060305 (2008).
 [16] M. Boissonneault, J. M. Gambetta, and A. Blais, Phys. Rev. A **79**, 013819 (2009).
 [17] D. H. Slichter, R. Vijay, S. J. Weber, S. Boutin, M. Boissonneault, J. M. Gambetta, A. Blais, and I. Siddiqi, Phys. Rev. Lett. **109**, 153601 (2012).
 [18] H. Haroche and J.-M. Raimond, *Exploring the Quantum: Atoms, Cavities, and Photons* (Oxford University Press, Oxford, 2006).
 [19] S. J. Srinivasan, N. M. Sundaresan, D. Sadri, Y. Liu, J. M. Gambetta, T. Yu, S. M. Girvin, and A. A. Houck, arXiv:1308.3471.
 [20] A. N. Korotkov, arXiv:1309.6405, Appendix B.
 [21] P. Meystre and M. Sargent III, *Elements of Quantum*

Optics (Springer-Verlag, Berlin, 2007).

- [22] H. J. Carmichael, Phys. Rev. Lett. **70**, 2273 (1993).
- [23] J. E. Johnson, C. Macklin, D. H. Slichter, R. Vijay, E. B. Weingarten, J. Clarke, and I. Siddiqi, Phys. Rev. Lett. **109**, 050506 (2012).
- [24] D. Riste, J. G. van Leeuwen, H.-S. Ku, K. W. Lehnert, and L. DiCarlo, Phys. Rev. Lett. **109**, 050507 (2012).
- [25] R. Barends, J. Kelly, A. Megrant, D. Sank, E. Jeffrey, Y. Chen, Y. Yin, B. Chiaro, J. Mutus, C. Neill, P. O'Malley, P. Roushan, J. Wenner, T. C. White, A. N. Cleland, and John M. Martinis, Phys. Rev. Lett. **111**, 080502 (2013).
- [26] Note that the language of the JC ladder of states in Fig. 2 corresponds to the full Hamiltonian (20) rather than the Hamiltonian (21) in the rotating frame.
- [27] A. Galiatdninov, A. N. Korotkov, and J. M. Martinis, Phys. Rev. A **85**, 042321 (2012).
- [28] J. Koch, T. M. Yu, J. Gambetta, A. A. Houck, D. I. Schuster, J. Majer, A. Blais, M. H. Devoret, S. M. Girvin, and R. J. Schoelkopf, Phys. Rev. A **76**, 042319 (2007).
- [29] J. Gambetta, A. Blais, M. Boissonneault, A. A. Houck, D. I. Schuster, and S. M. Girvin, Phys. Rev. A **77**, 012112 (2008).
- [30] B. R. Mollow, Phys. Rev. **188**,1969 (1969).